ANGULAR MOMENTUM AND THE COLLECTIVE MODES EXCITED IN DEEP-INELASTIC PROCESSES AND IN FISSION

L. G. Moretto

Lawrence Berkeley Laboratory
University of California
Berkeley, California 94720

ABSTRACT

The angular momentum effects in deep inelastic processes and fission have been studied in the limit of statistical equilibrium. The model consists of two touching liquid drop spheres. Angular momentum fractionation has been found to occur along the mass asymmetry coordinate. Thermal excitation of fragment spin is predicted to occur in the degrees of freedom which can bear angular momentum, like wriggling, tilting, bending, and twisting.

INTRODUCTION

The importance of angular momentum in recent studies is illustrated by the work on gamma-ray multiplicities [1-8], gamma-ray angular distributions [9], and alpha [10] and sequential fission probabilities and angular distributions [11-13]. All of these topics have as a major theme the angular momentum and its partitioning among several, though not necessarily yet identified, degrees of freedom.

Transport equations have been advocated for the description of the time evolution of the intermediate complex formed in heavy-ion collisions and have even been applied with moderate success to the angular momentum transfer observed in these reactions [14-16]. A good deal can be learned by considering a very simple model, striving to obtain transparent analytical results and by considering the long time limit of statistical equilibrium, to which all the transport equations must tend.

The statistical equilibrium limit is not deprived of interest. On the one hand, such a limit applies to all of the compound nucleus processes, fission in particular. On the other hand, many of the collective degrees of freedom which we consider are quite likely to be in most cases, either close, or at the statistical equilibrium limit. There are, of course, most interesting and notable exceptions. In what follows, we are going to consider explicitly the mass asymmetry coordinates, the wriggling, tilting and bending modes.

ANGULAR MOMENTUM FRACTIONATION ALONG THE MASS ASYMMETRY COORDINATE

Variations in the total exit channel angular momentum along the mass asymmetry coordinate have been observed in non-equilibrium heavy-ion reactions [5]. In these processes the angular momentum fractionation appears to arise mainly from the decreasing rate of spread of the population along the mass asymmetry coordinate with increasing angular momentum due to the dependence of the interaction time upon angular momentum.

Angular momentum fractionation is expected even when statistical equilibrium is attained along the mass asymmetry mode, either directly as the end product of diffusion, or through population from compound nucleus. The reason for this can easily be seen. The potential as a function of mass asymmetry (ridge potential) has a minimum at symmetry with the second derivative increasing with increasing angular momentum. At equilibrium, the mass distributions for large angular momenta are more sharply peaked about symmetry than the mass distributions for small angular momenta. It follows that, after summation over all partial ℓ-waves the angular momentum decreases with increasing symmetry. More quantitatively, let us consider the ridge line as a function of mass asymmetry and angular momenta. For two touching liquid drop spheres, of mass numbers A_1, A_2, and for small values of $y = \frac{1}{2}(A_1-A_2)/(A_1+A_2)$, the energy is

$$E = (0.45354 + 1.29584\ y^2)E_R + (0.89244 + 0.46664\ y^2)E_C + (1.25992 - 0.55996\ y^2)E_S = \alpha E_R + \beta E_C + \gamma E_S \quad ,$$

where E_R, E_C, E_S are the rotational, Coulomb, and surface energies of the equivalent sphere.

Now let us assume that a compound nucleus has been formed and that neutron decay and fission are the only competing processes. In the constant temperature limit, dropping ℓ-independent factors and assuming $\Gamma_T \cong \Gamma_N$, we get for the distribution in ℓ and y:

$$P(\ell,y) \propto \frac{\Gamma_F}{\Gamma_N}(\ell,y) \propto \ell\, e^{-(R E_R + C E_C + S E_S)/T}\, d\ell\, dy \quad ,$$

where $R = \alpha-1$, $C = \beta-1$, $S = \gamma-1$, and ℓ is the angular momentum. Integrating over angular momentum we obtain

$$P(y) \propto \frac{T}{\mathcal{R} E_R^{mx}} \left\{ \exp - \frac{C E_C + S E_S}{T} \right\} \left\{ \exp \mathcal{R} \frac{E_R^{mx}}{T} - 1 \right\} \quad ,$$

where E_R^{mx} is the maximum rotational energy of the equivalent sphere, and $\mathcal{R} = -R$. The first moment of the angular momentum is

$$\bar{\ell}(y) = \ell_{mx} \frac{\left[1 - \sqrt{\frac{T}{R E_R^{mx}}}\ F\left(\sqrt{\frac{\mathcal{R} E_R^{mx}}{T}} \right) \right] \exp \frac{\mathcal{R} E_R^{mx}}{T}}{\exp \frac{\mathcal{R} E_R^{mx}}{T} - 1} \quad ,$$

where E_R^{mx} is the maximum rotational energy of the equivalent sphere, $F(x)$ is the Dawson's integral and $\mathcal{R} = -R$. The second moment of the angular momentum is:

$$\bar{\ell}^2(y) = \ell_{mx}^2 \frac{\left(1 - \frac{T}{\mathcal{R} E_R^{mx}} \right) \exp \frac{\mathcal{R} E_R^{mx}}{T} + \frac{T}{\mathcal{R} E_R^{mx}}}{e^{\mathcal{R} E_R^{mx}/T} - 1} \quad .$$

These moments as well as the mass distributions, as a function of the mass asymmetry y are shown in Fig. 1(a,b).

The interpretation of Fig. 1(b), which depicts $\bar{\ell}$ and $\overline{\ell^2}$ as a function of y is fairly straightforward. For moderate values of y, both $\bar{\ell}/\bar{\ell}_D$ and $\overline{\ell^2}/\overline{\ell^2_D}$ are constant and close to unity. This is due to the fact that the high ℓ-waves dominate the yield for this range of asymmetries, so that averaging over ℓ yields a value of $\bar{\ell}$, $\overline{\ell^2}$, which is essentially $\bar{\ell}_D, \overline{\ell^2_D}$. However, the mass distributions for high ℓ-waves are relatively narrow, and as one moves out to greater asymmetries their contribution to the total yield for a given asymmetry becomes less important, resulting in a lower average ℓ.

At the expense of an analytic answer, a more accurate picture can be obtained by including the angular momentum dependence of Γ and by replacing Γ_n with $\Gamma_T = \Gamma_n + \Gamma_f$. The results are shown in Figs. 2(a,b). The qualitative interpretation is similar to that described above: $\bar{\ell}, \overline{\ell^2}$ are nearly constant as a function of y for small y due to the dominance of the high ℓ waves, and then drop off rather abruptly because of the small contribution of the high ℓ-waves to the extreme asymmetries.

Another case which may be relevant in heavy-ion reactions arises when the system equilibrates along the ridge line and decays without passing through the compound nucleus stage. In other words, there is no competition from neutron emission or from other particle decay modes.

Calculations without neutron competition are shown in Fig. 3(a,b). The mass distributions for the individual ℓ-waves shown in Fig. 3(a) are identical to those in Fig. 2(a) since the effect of neutron competition only changes the normalization. However, the distribution P(y) is now considerably broader than its counterpart in Fig. 2(a) due to the change in the weighting of $P(\ell,y)$ in the integration over ℓ.

The most significant effect of the assumption of equilibration along the ridge line can be seen in Fig. 3(b). In contrast to the preceding case (neutron competition), $\bar{\ell}$ and $\overline{\ell^2}$ peak at symmetry and fall off substantially with increasing y. The dramatic differences in the ℓ-fractionation imply that it may be possible to distinguish between the two mechanisms, i.e., compound nucleus fission and non-compound nucleus decay, by measuring the angular momentum as a function of asymmetry.

STATISTICAL COUPLING BETWEEN ORBITAL AND INTRINSIC ANGULAR MOMENTA AND WRIGGLING MODES

Let us assume that we can approximate the exit channel configuration by two touching, equal, rigid spheres with all the associated rotational degrees of freedom. This model leads to simple analytical predictions for the relevant statistical distributions.

First, let us consider the equilibrium between intrinsic rotation of the fragment and their orbital rotation, assuming that the relevant angular momenta are all parallel to each other. If the total angular momentum is I and the spin fragment is s, the energy, for an arbitrary partition between orbital and intrinsic angular momentum is:

$$E(s) = \frac{(I-2s)^2}{2\mu r^2} + \frac{2s^2}{2\mathcal{I}} = \left(\frac{2}{\mu r^2} + \frac{1}{\mathcal{I}}\right) s^2 - \frac{2I}{\mu r^2} s + \frac{I^2}{2\mu r^2} \quad .$$

The first term is the orbital and the second the intrinsic rotational

energy, $\mathcal{J}$ being the moment of inertia of one of the two equal spheres. The average spin per fragment $\bar{s}$ is given by

$$2\bar{s} = \frac{\int s\, e^{-E(s)/T}\, ds}{Z} = \frac{2\mathcal{J}}{\mu r^2 + 2\mathcal{J}} I = \frac{2}{7} I = 2I_R \quad .$$

where Z is the partition function. The second moment $\overline{s^2}$ is given by:

$$4\overline{s^2} = \frac{2\mu r^2 \mathcal{J} T}{(\mu r^2 + 2\mathcal{J})} + \frac{4I^2\mathcal{J}^2}{(\mu r^2 + 2\mathcal{J})^2} \quad .$$

From this we obtain the standard deviation

$$4\sigma_s^2 = \frac{2\mu r^2 T}{(\mu r^2 + 2\mathcal{J})} = \frac{10}{7}\mathcal{J}T \quad .$$

The quantity $4\sigma_s^2$ represents the amount of angular momentum trade-off allowed by the temperature between orbital and intrinsic rotation.

In some instances, such as gamma-multiplicity measurements, one is interested in the average sum of the moduli of the fragment spins. This can be obtained as

$$2|\bar{s}| = \int |s|\; e^{-E(s)/T}\, \frac{ds}{Z} \quad ,$$

which yields, in dimensionless form:

$$\frac{2|\bar{s}|}{\sqrt{\mathcal{J}^* T}} = 2\left[\frac{1}{\sqrt{\pi}} \exp(-x^2) + x\,\mathrm{erf}(x)\right] \quad ,$$

where $x = I_R/\sqrt{\mathcal{J}^* T}$ and $\mathcal{J}^* = \mu r^2 \mathcal{J}/(\mu r^2 + 2\mathcal{J})$. Also $I_R = 1/7$ is the spin per fragment arising from rigid rotation. The above expression is plotted in Fig. 4. In the limit of large I, one obtains

$$2|\bar{s}| = \frac{2\mathcal{J}I}{\mu r^2 + 2\mathcal{J}} = \frac{2}{7} I \quad .$$

For small I,

$$\frac{2|\bar{s}|}{\sqrt{\mathcal{J}^* T}} \cong \frac{2}{\sqrt{\pi}} (1 + x^2) \quad ,$$

to order x^2, so for I=0 one obtains

$$2|\bar{s}| = 2\sqrt{\frac{\mathcal{J}T}{\pi}} \left(\frac{\mu r^2}{\mu r^2 + 2\mathcal{J}}\right)^{1/2} = 2\sqrt{\frac{5\mathcal{J}T}{7\pi}} \quad .$$

In this case the fragment angular momentum at zero angular momentum arises from the excitation of a collective mode (wriggling [17]) in which the two fragments spin in the same direction while the system as a whole rotates in the opposite direction in order to maintain I=0.

Contrary to what has been assumed thus far, the wriggling mode is actually doubly degenerate, as illustrated in Fig. 5. Let us now couple this doubly degenerate mode to the spin arising from rigid rotation. If the aligned component of the angular momentum arising from rigid rotation is I_R and that due to wriggling is R, the total angular momentum for each fragment is

$$s^2 = I_R^2 + R^2 + 2I_R R\cos\theta \quad ,$$

and the total energy is

$$E = \frac{35I_R^2 + 14R^2}{10\mathcal{J}} \quad .$$

The angular momentum of either fragment is

$$s = \sqrt{I_R^2 + R^2 + 2I_R R\cos\theta} \quad ,$$

so the average sum of the moduli of the fragment spins is

$$2|\bar{s}| = \frac{2}{Z}\int\sqrt{I_R^2 + R^2 + 2I_R R\cos\theta}\; R\exp(-E/T)dRd\theta \quad .$$

A rather accurate approximation to $2|\bar{s}|$ is given in dimensionless form by:

$$\frac{2|\bar{s}|}{\sqrt{\mathcal{J}^*T}} = 2x + \frac{1}{2x} - \frac{1}{2}\left(x + \frac{1}{x}\right)\exp(-x^2) + \sqrt{\pi}\left(1 + \frac{x^2}{2}\right)\mathrm{erfc}(x) \quad .$$

This function, which is plotted in Fig. 4, has the following limiting values:

$$\frac{2|\bar{s}|}{\sqrt{\mathcal{J}^*T}} = \sqrt{\pi}\left(1 + \frac{x^2}{2}\right) \quad , \qquad \text{small } I_R$$

$$\frac{2|\bar{s}|}{\sqrt{\mathcal{J}^*T}} = 2x + \frac{1}{2x} \quad , \qquad \text{large } I_R \quad .$$

Also in the limit of large I_R, one obtains

$$4\sigma^2 = 4I_R^2 + 4\overline{R^2} - 4I_R^2 - 2\overline{R^2} = 2\overline{R^2} = 2\mathcal{J}^*T \quad .$$

It is interesting to note that the wriggling mode generates a random angular momentum in a plane perpendicular to the line of centers of the fragments.

THERMAL FLUCTUATION OF THE ANGULAR MOMENTUM PROJECTION ON THE DISINTEGRATION AXIS: TILTING

Above we have assumed that the two touching fragments are aligned with their common axis perpendicular to the total angular momentum. Because of the thermal fluctuations, this condition can be relaxed (see Fig. 5). Assuming now that the two fragments are rigidly attached one to the other, the energy is given by

$$E = \frac{I^2 - K^2}{2\mathcal{I}_\perp} + \frac{K^2}{2\mathcal{I}_\parallel} = \frac{I^2}{2\mathcal{I}_\perp} + \frac{K^2}{2\mathcal{I}_{eff}}$$

where: $\mathcal{I}_\perp = 2\mathcal{I} + \mu r^2$; $\mathcal{I}_\parallel = 2\mathcal{I}$; and $\mathcal{I}_{eff}^{-1} = \mathcal{I}_\parallel^{-1} - \mathcal{I}_\perp^{-1}$; K is the projection of the angular momentum I along the line of centers. One can easily obtain

$$\overline{K^2} = \mathcal{I}_{eff}\, T = \frac{14}{5}\mathcal{I}T \quad .$$

The averaged square spin is

$$4\overline{s^2} = \overline{K^2} + \frac{4}{49} I^2 - \frac{4}{49}\overline{K^2} = \frac{45}{49}\overline{K^2} + \frac{4}{49} I^2$$

The average spin, on the other hand, is:

$$2|\bar{s}| \cong \frac{2}{7} I + \frac{45}{28}\frac{\overline{K^2}}{I} = \frac{2}{7} I \left(1 + \frac{45}{8}\frac{\overline{K^2}}{I^2}\right) = \frac{2}{7} I + \frac{9}{2}\frac{\mathcal{I}T}{I}$$

where we have dropped terms of order higher than $\overline{K^2}/I^2$.

Due to the excitation of this mode the reaction plane is not perpendicular to the total angular momentum of the system I, but is "tilted" by an angle θ_t given by: $\sin\theta_t = \sqrt{\overline{K^2}/I^2}$. The angle more relevant to sequential fission angular distributions is the angle between the total spin of one fragment and the normal to the line of centers (in the same plane as I), which is given by: $\sin\theta = \sqrt{\overline{K^2}/4\overline{s^2}}$. Since I is considerably larger than $\bar{s}$, this angle can be considerably larger than θ_t. The combined effect of wriggling and tilting will produce spin components along all the coordinate axes. If the separation axis is the z-axis, tilting will lead to an rms z-component of $\sqrt{\overline{K^2}/4} = 0.84\sqrt{\mathcal{I}T}$ for each fragment. On the other hand, the average x- and y-components will be $\sqrt{\overline{R^2}/2} = 0.60\sqrt{\mathcal{I}T}$; hence, tilting and wriggling together generate an angular momentum which is almost random.

TWISTING AND BENDING MODES [17] EXCITED IN A ZERO ANGULAR MOMENTUM SYSTEM

These three degrees of freedom are illustrated in Fig. 6. They are degenerate in our two-equal-sphere model [12]. If R is the angular momentum of each fragment, we obtain

$$\bar{R} = \frac{2}{\sqrt{\pi}}(\mathcal{I}T)^{\frac{1}{2}} \quad ,$$

$$\overline{R^2} = \frac{3}{2}\mathcal{I}T$$

and

$$\sigma_R^2 = \left(\frac{3}{2} - \frac{4}{\pi}\right)\mathcal{I}T \cong 0.227\,\mathcal{I}T \quad .$$

COUPLING OF TWISTING AND BENDING MODES TO RIGID ROTATION

We want to generalize the previous calculation to the case of non-zero total angular momentum. Let us assume that each fragment has an aligned angular momentum component I_R arising from rigid rotation and a random component R due to the bending and twisting modes. The overall rotational energy arising from the fragment spins is:

$$E = \frac{1}{\mathcal{J}} (I_R^2 + R^2) \quad .$$

The average total angular momentum of the fragments, in dimensionless form, is:

$$\frac{2|\bar{s}|}{\sqrt{\mathcal{J}T}} = \left(2x + \frac{1}{x}\right) \mathrm{erf}(x) + \frac{2}{\sqrt{\pi}} \exp(-x^2) \quad ,$$

where $x = I_R/\sqrt{\mathcal{J}T}$. This function is plotted in Fig. 7. For small x one obtains

$$\frac{2|\bar{s}|}{\sqrt{\mathcal{J}T}} \cong \frac{4}{\sqrt{\pi}} \left(1 + \frac{x^2}{3}\right) \quad .$$

In the limit of $I_R = 0$, one obtains

$$2|\bar{s}| = \frac{4}{\sqrt{\pi}} \sqrt{\mathcal{J}T} = 2\bar{R} \quad .$$

in agreement with the results of the last section. For large x,

$$\frac{2|\bar{s}|}{\sqrt{\mathcal{J}T}} \cong 2x + \frac{1}{x}$$

or

$$2|\bar{s}| = 2I_R + \frac{\mathcal{J}T}{I_R} = 2I_R + \frac{2}{3} \frac{\overline{R^2}}{I_R} = \frac{2}{7} I \left(1 + \frac{49}{2} \frac{\mathcal{J}T}{I^2}\right) \quad .$$

Similarly the average square angular momentum to order $\overline{R^2}/I_R$ yields

$$4\overline{s^2} = 4(I_R^2 + \overline{R^2})$$

$$\sigma^2 = \frac{4}{3} \overline{R^2} = 2\mathcal{J}T \quad .$$

CONCLUSION

Using a simple model we have investigated the angular momenta associated with a number of collective degrees of freedom. For the mass asymmetry mode we have found that there is an appreciable ℓ-fractionation along the mass asymmetry coordinate, even in the equilibrium limit. Furthermore, the distinctly different patterns observed for the case of compound nucleus decay and for non-compound nucleus decay (i.e., equilibration along the ridge line) imply that it may be possible to experimentally distinguish between these two mechanisms, perhaps via gamma-ray multiplicity measurements. Six other collective modes have been considered: two wriggling, one tilting, two bending, and one twisting. Excitation of these modes causes a modest increase in the average fragment spins over the rigid rotational value but lead to a sizeable spread in the fragment's angular momenta about the average value.

REFERENCES

[1] R.Albrecht, W.Dünnweber, G.Graw, H.Ho, S.A.Steadman, and J.P.Wurm, Phys. Rev. Lett. 34, 1500 (1975).
[2] M.Ishihara, J.Numao, T.Fukada, K.Tanaka, and T.Inamura, Proceedings of the Symposium on Macroscopic Features of Heavy-Ion Collisions, Argonne, Illinois, 1976, edited by D.G.Kovar, ANL Report No. ANL-PHY-76, p.617.
[3] P.Glässel, R.S.Simon, R.M.Diamond, R.C.Jared, I.Y.Lee, L.G.Moretto, J.O.Newton, R.Schmitt, and F.S.Stephens, Phys. Rev. Lett. 38, 331 (1977).
[4] M.Berlanger, M.A.Deleplanque, C.Gerschel, F.Hanappe, M.LeBlanc, J.F.Mayault, C.Ngô, D.Paya, N.Perrin, J.Péter, B.Tamain, and L.Valentin, J. Phys. Lett. L37, 323 (1976).
[5] M.M.Aleonard, G.J.Wozniak, P.Glässel, M.M.Deleplanque, R.M.Diamond, L.G. Moretto, R.P.Schmitt, and F.S.Stephens, Phys. Rev. Lett. 40, 622 (1978).
[6] J.B.Natowitz, M.N.Namboordiri, P.Kasiraj, R.Eggers, L.Alder, P.Gouthier, C.Cerruti, and T.Alleman, Phys. Rev. Lett. 40, 751 (1978).
[7] P.R.Christensen, F.Folkmann, O.Hansen, O.Nathan, N.Trautner, F.Videbaek, S.Y.van der Werf, H.C.Britt, R.P.Chestnut, H.Freiesleben, and F. Pühlhofer, Phys. Rev. Lett. 40, 1245 (1978).
[8] A.Olmi, H.Sann, D.Pelte, Y.Eyal, A.Gobbi, W.Kohl, U.Lynen, G.Rudolf, H.Stelzer, and R.Bock, Phys. Rev. Lett. 41, 688 (1978).
[9] R.A.Dayras, R.G.Stokstad, C.B.Fulmer, D.C.Hensley, M.L.Halbert, R.L. Robinson, A.H.Snell, D.G.Sarantites, L.Westerberg, and J.H.Barber, Phys. Rev. Lett. 42, 697 (1979).
[10] H.Ho, R.Albrecht, W.Dünnweber, G.Graw, S.G.Steadman, J.P.Wurm, D.Disdier, V.Rauch, and F.Scheibling, Z. Physik A283, 234 (1977).
[11] P.Dyer, R.J.Puigh, R.Vandenbosch, T.D.Thomas, and M.S.Zisman, Phys. Rev. Lett. 39, 392 (1977).
[12] G.J.Wozniak, R.P.Schmitt, P.Glässel, R.C.Jared, G.Bizard, and L.G. Moretto, Phys. Rev. Lett. 40, 1436 (1978).
[13] H.J.Specht, Proceedings of the International Conf. on Nuclear Interactions, Australian Academy of Science, Canberra City, Australia, 8/28-9/2, 1978
[14] R.Regimbart, A.N.Behkami, G.J.Wozniak, R.P.Schmitt, J.S.Sventek, and L.G.Moretto, Phys. Rev. Lett. 41, 1355 (1978)
[15] G.Wolschin and W.Nörenberg, Phys. Rev. Lett. 41, 691 (1978).
[16] S.Ayik, G.Wolschin and W.Nörenberg, Z. Physik A286, 271 (1978).
[17] J.R.Nix and W.J.Swiatecki, Nucl. Phys. 71, 1 (1965).

FIGURE CAPTIONS

Fig. 1. (a) Mass distributions for the indicated reaction obtained by integrating over all ℓ-waves leading to fission (squares) and for selected individual ℓ-waves (solid curves). The ℓ-values are ℓ=0, $\ell_{mx}/2$, and ℓ_{mx}. All curves have been normalized to unity at symmetry. (b) Mean (crosses) and mean squared (squares) angular momentum divided by the corresponding quantities obtained by averaging over the ℓ-distribution which leads to fission vs. asymmetry.

Fig. 2. (a) Same as Fig. 1(a) except that the angular momentum dependence of the temperature and total reaction width have been incorporated into the calculations (see text). (b) Same as Fig. 1(b) but including the same refinements as the calculation shown in Fig. 2(a).

Fig. 3. (a) Same as Fig. 2(a) but in the absence of neutron competition. Note that only the total mass distribution (squares) is different from Fig. 2(a). (b) Same as Fig. 2(b) but without neutron competition.

Fig. 4. Total spin of the fragments arising from wriggling as a function of the spin arising from rigid rotation alone plotted in dimensionless form. The upper solid curve shows the result for both of the wriggling modes while the lower solid curve corresponds to the excitation of a single wriggling mode (see text). The limiting behavior for both small and large x are indicated in both cases.

Fig. 5. Schematic illustration of the tilting mode and the doubly degenerate wriggling modes for the two equal sphere model. The long arrows originating at the point of tangency for the two spheres is the orbital angular momentum while the shorter arrows represent the individual fragment spins.

Fig. 6. Schematic illustration of the twisting and bending modes for the two equal sphere model. Note the pairwise cancellation of the fragment spins.

Fig. 7. Total fragment spin as a function of the spin arising from rigid rotation for the twisting and bending modes. Dimensionless forms are utilized. The limiting behavior for large and small x are indicated.

This work was supported by the U. S. Department of Energy under Contract W-7405-ENG-48.

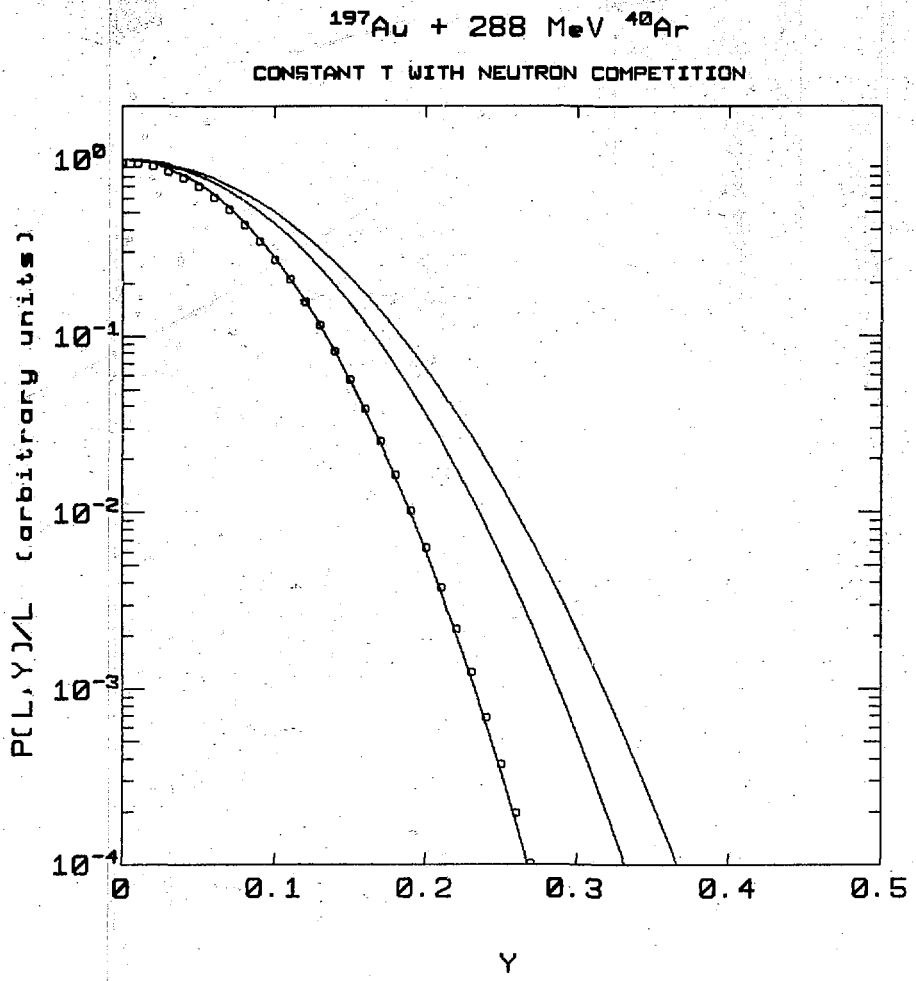

XBL 794-9200

Figure 1a

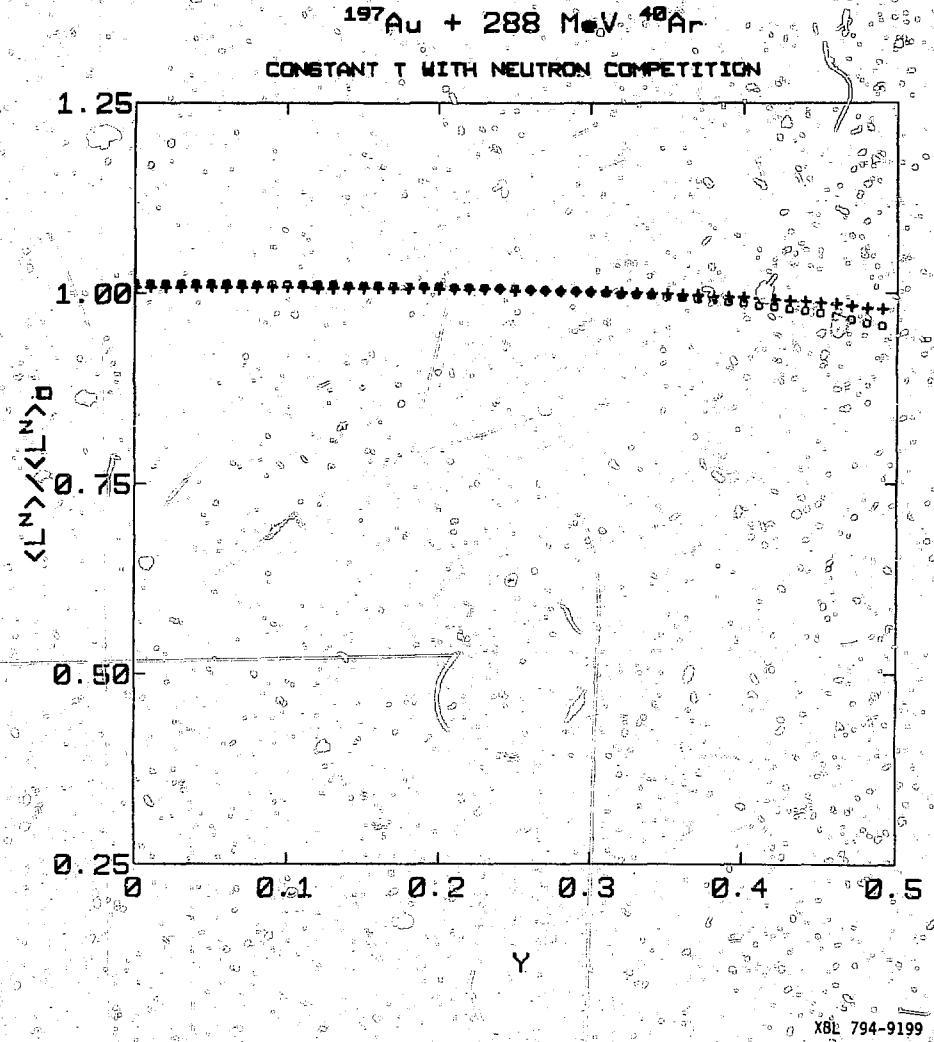
^{197}Au + 288 MeV ^{40}Ar
CONSTANT T WITH NEUTRON COMPETITION
1.25
1.00
0.75
0.50
0.25
$\langle L^N \rangle / \langle L^N \rangle_0$
0
0.1
0.2
0.3
0.4
0.5
Y
XBL 794-9199

Figure 1b

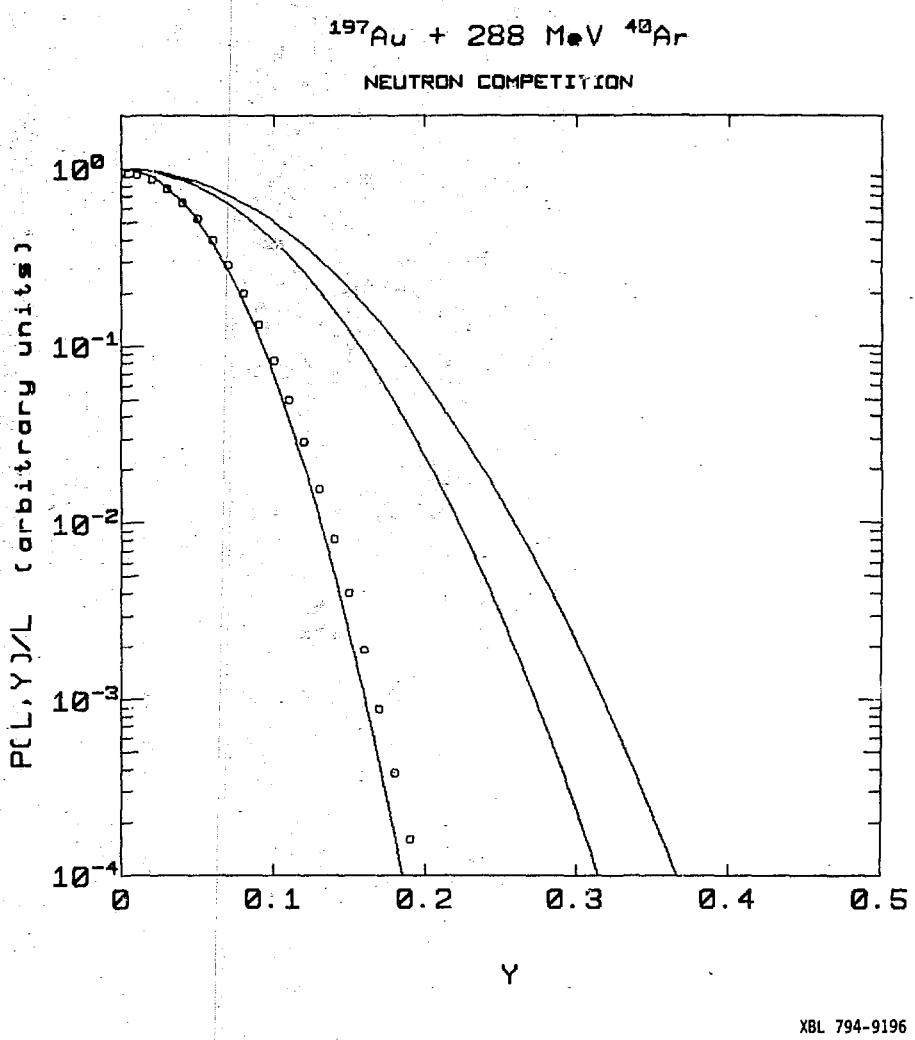
197Au + 288 MeV 40Ar
NEUTRON COMPETITION
P[L,Y]/L (arbitrary units)
10^0
10^-1
10^-2
10^-3
10^-4
0
0.1
0.2
0.3
0.4
0.5
Y
XBL 794-9196

Figure 2a

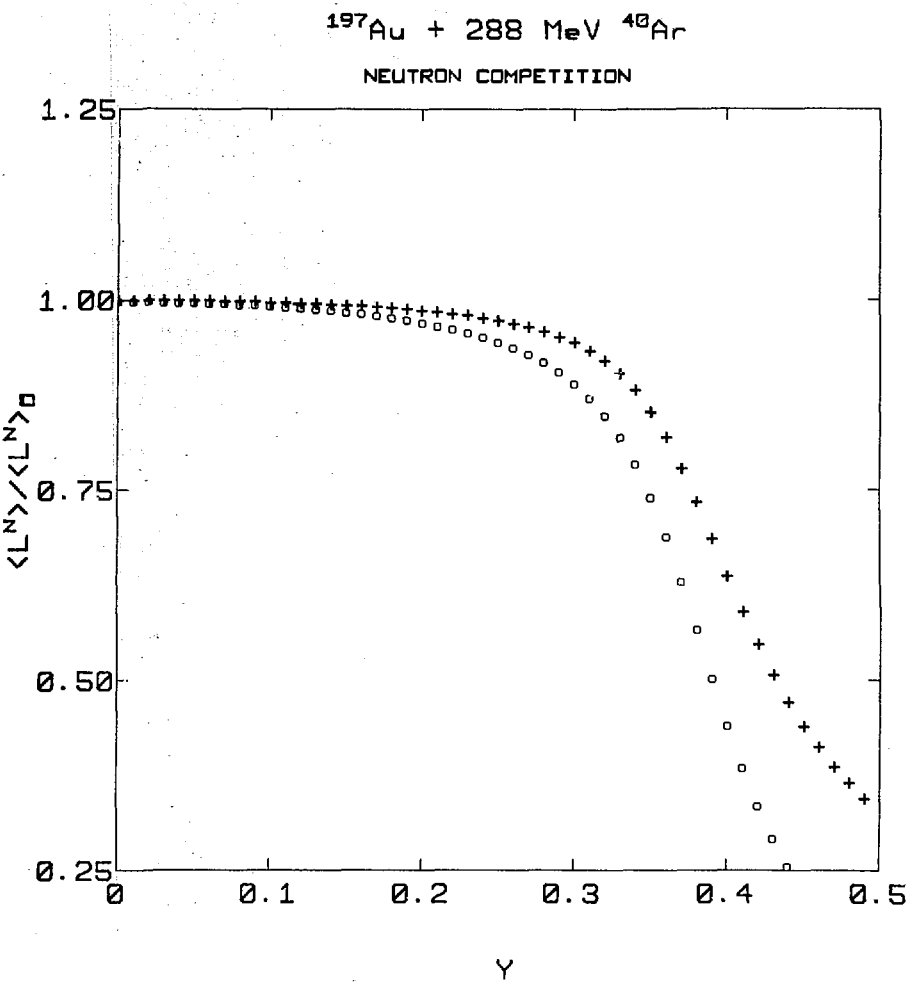

XBL 794-9198

Figure 2b

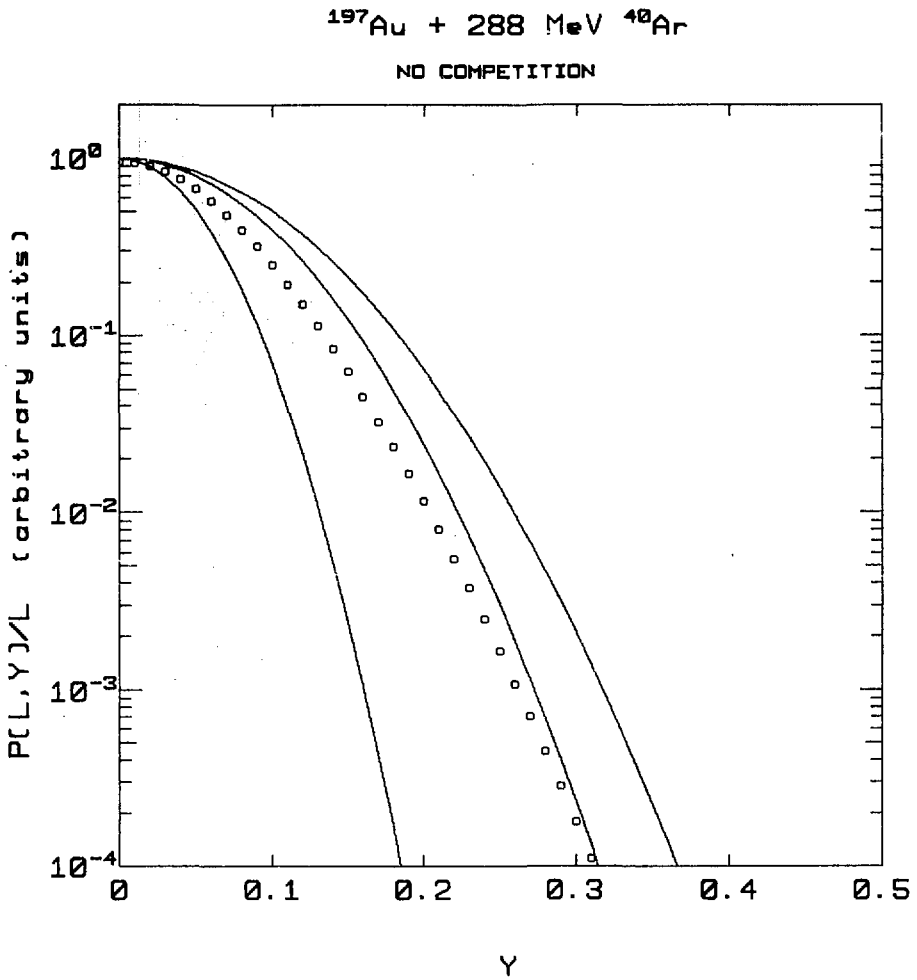

XBL 794-9195

Figure 3a

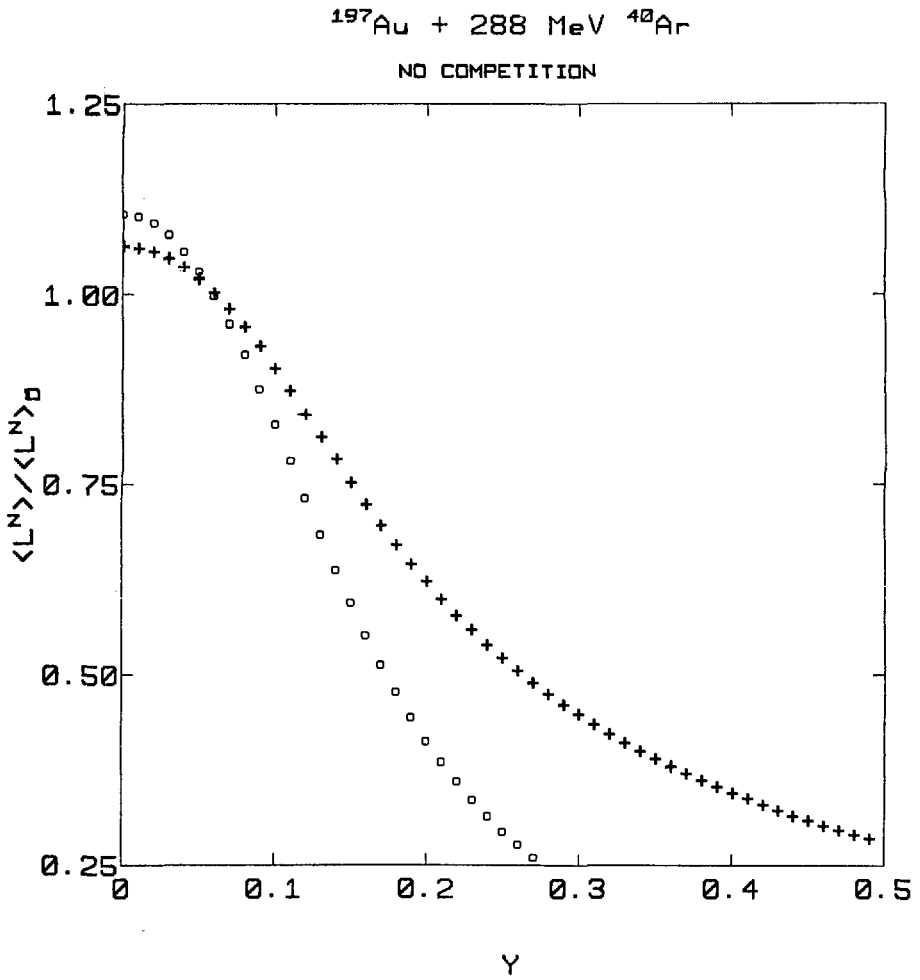

XBL 794-9197

Figure 3b

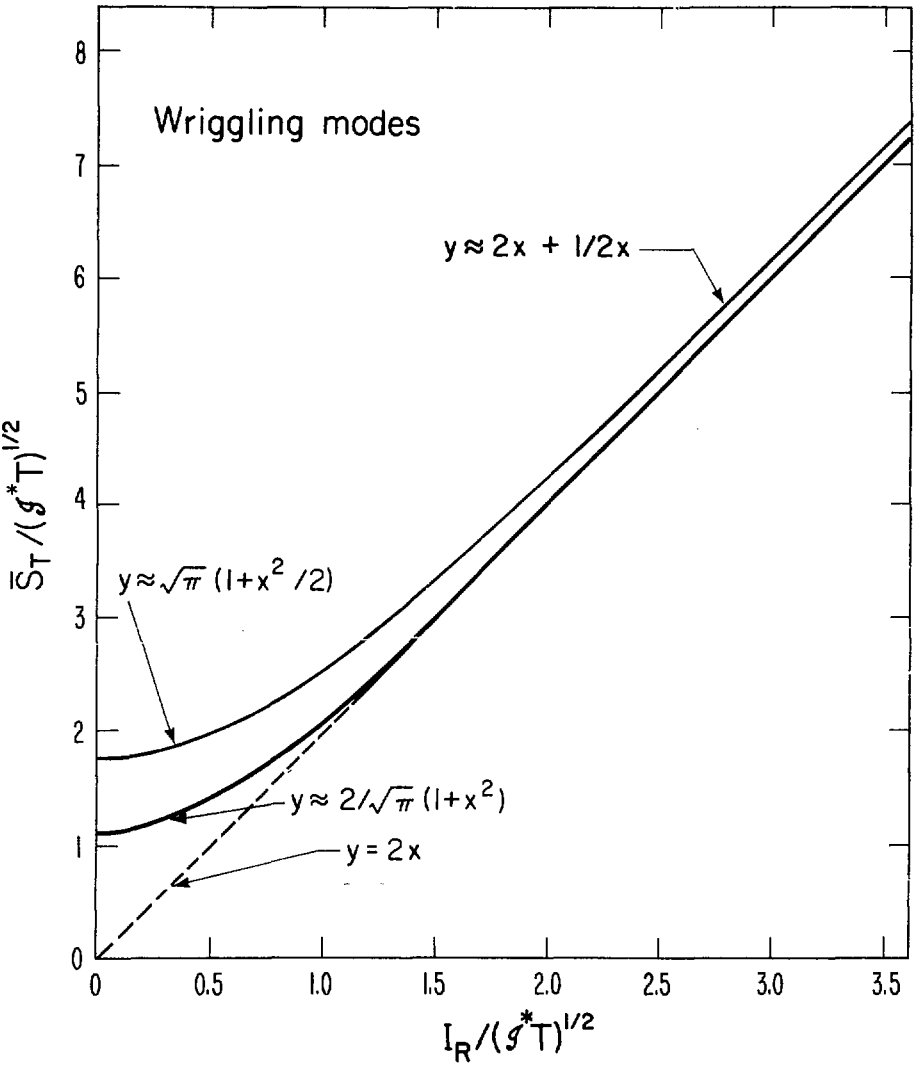

XBL 793 - 822

Figure 4

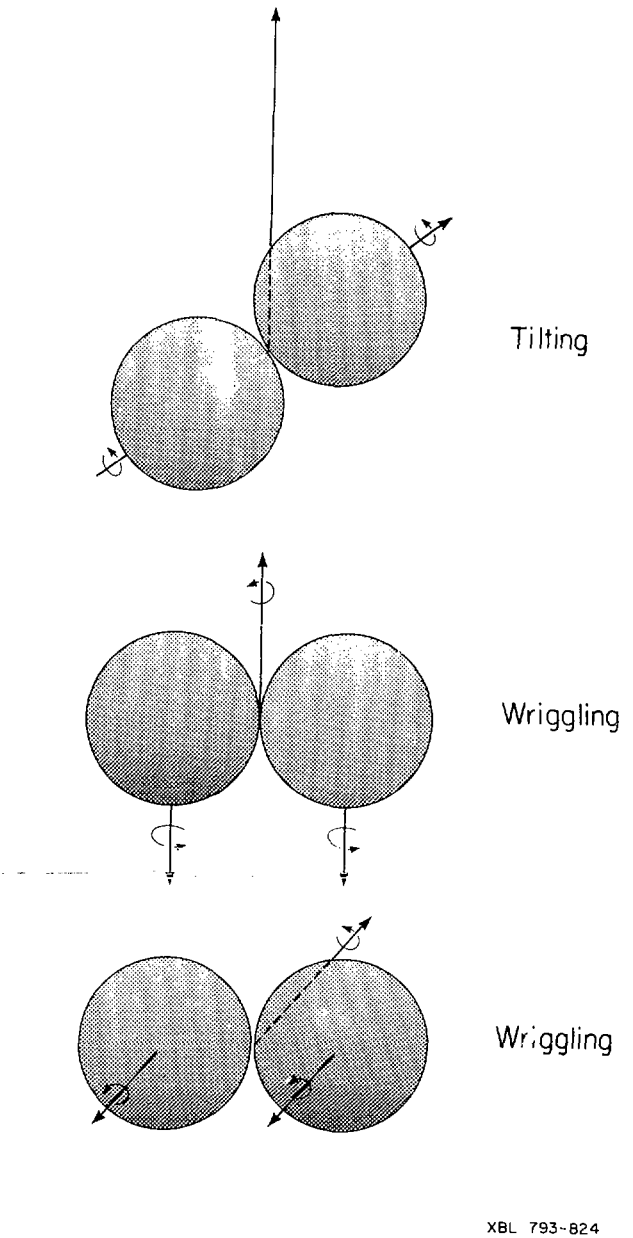

XBL 793-824

Figure 5

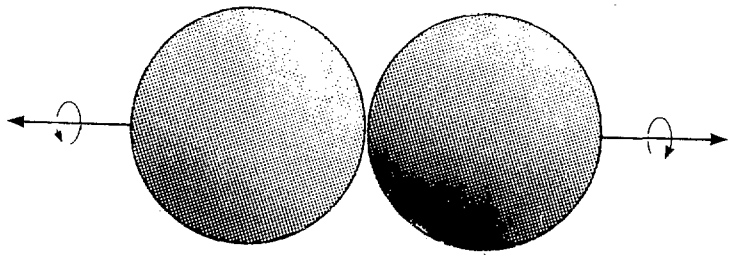

Twisting

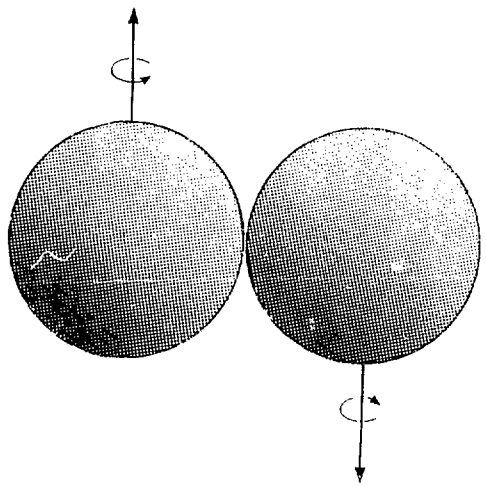

Bending

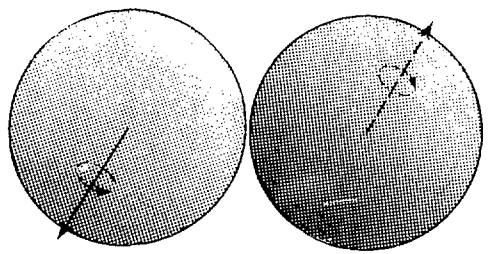

Bending

XBL 791-206

Figure 6

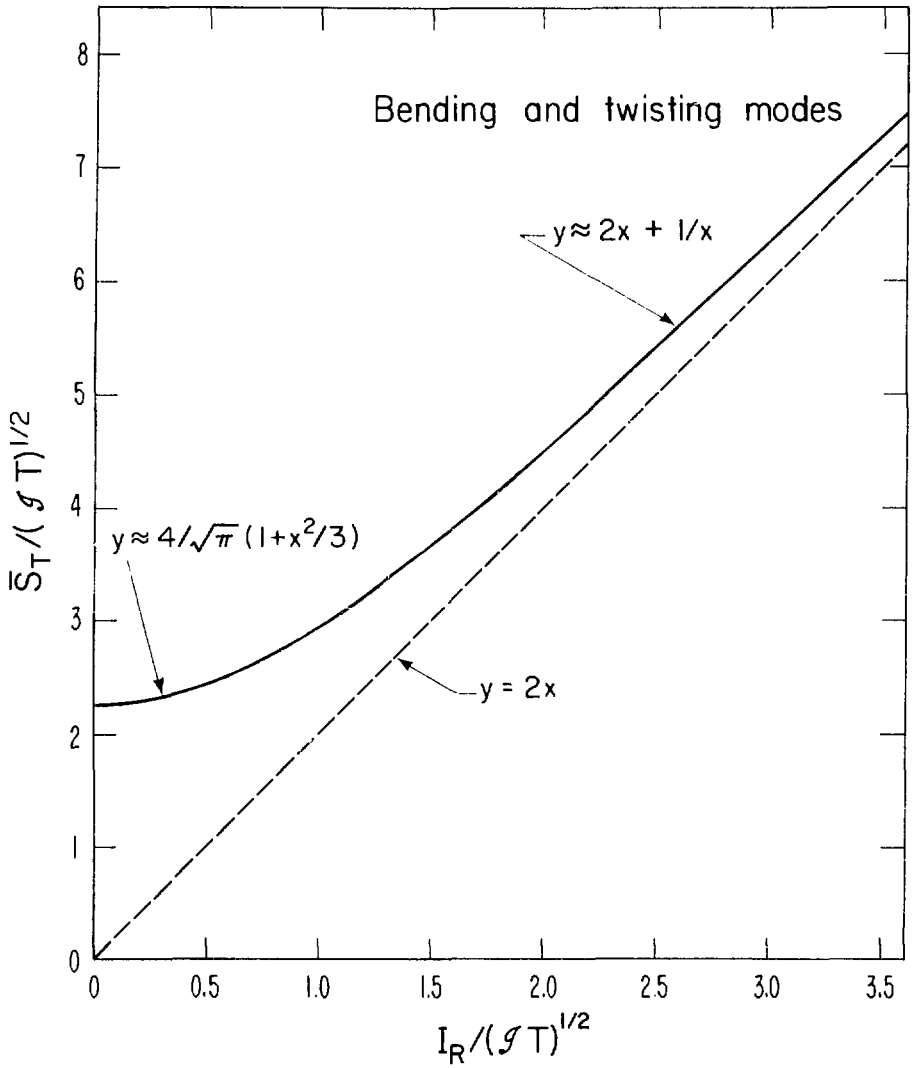

XBL 793-823

Figure 7